

Measurement-based quantum machine learning

Luis Mantilla Calderón^{1,2,*}, Polina Feldmann^{3,4,†}, Robert Raussendorf^{4,5}, and Dmytro Bondarenko^{3,4,‡}

¹*Department of Computer Science, University of Toronto, Canada*

²*Vector Institute for Artificial Intelligence, Toronto, Canada*

³*Department of Physics & Astronomy, University of British Columbia, Vancouver, Canada*

⁴*Stewart Blusson Quantum Matter Institute, University of British Columbia, Vancouver, Canada and*

⁵*Institut für Theoretische Physik, Leibniz Universität Hannover, Hannover, Germany*

(Dated: May 15, 2024)

A quantum neural network (QNN) is an object that extends the notion of a classical neural network to quantum models for quantum data. We can create a QNN by parametrizing a quantum process and then using it to model unknown relations between quantum states. In this paper, we explore how to use measurement-based quantum computation for quantum machine learning problems and propose a universal QNN in this framework which we call the multiple-triangle ansatz (MuTA). Using the proposed QNN, we solve several tasks, including learning a universal set of gates, optimizing measurement with post-processing, learning a quantum instrument, and the classification of classical data. Finally, we discuss how to train an ansatz under the hardware constraints imposed by photonic Gottesman-Kitaev-Preskill qubits. Our work demonstrates the feasibility of using measurement-based quantum computation as a framework for quantum machine learning algorithms.

I. INTRODUCTION

The idea of building a quantum computer has led to the development of several algorithms that bring significant speedups over their classical counterparts. Famous examples include Shor’s algorithm, Grover’s algorithm, and quantum simulation algorithms, which outperform current classical algorithms in the large-scale limit. However, these algorithms require a large number of qubits and gates with the addition of quantum error correction to be implemented, which is a big challenge for current quantum hardware. Thus, it is of interest to find algorithms that can be implemented with fewer resources and still bring speedups over classical algorithms.

One approach to save resources in some problems is using measurements with feedback. This has been shown to bring significant resource savings in several algorithms, such as implementing Shor’s algorithm with fewer qubits [1], preparing the ground state of the toric code [2], and preparing matrix product states (MPS) with exponentially fewer qubits than the counterpart with no measurement plus feedback [3]. This resource saving is one of the many reasons why measurement-based quantum computation (MBQC) [4] is of interest to this field.

Moreover, another idea that has been explored recently is quantum machine learning (QML) [5]. The primary objective of QML is to use current quantum hardware, capable of implementing parametrized gates natively, as machine learning models for performing inference over datasets of interest. One of the key aims is to find a quantum advantage in these models before reaching fault-tolerant systems. Current literature, including works like [6–10], has shown some evidence of utility in quantum

neural networks, but it is still unclear if they can bring a significant advantage over classical algorithms. Beyond its potential for a computational advantage over classical approaches, QML is inherently valuable, offering novel approaches to problem-solving and potential applications in fields where analysis of quantum data is required.

In this paper, we aim to study a family of models that harness both quantum and classical resources to process classical and quantum data. Our approach utilizes measurement-based quantum computation as a framework to define quantum neural networks. This concept has been previously explored in the context of the variational quantum eigensolver [11], multi-class classification [12], and generative modeling [13]. In Section II, we propose a methodology for creating QML models in MBQC. Additionally, Section III, introduces a universal quantum neural network architecture that has several desired properties for a QNN and can be used to solve a wide range of tasks. We call this QNN architecture the multiple-triangle ansatz (MuTA). In Section IV we demonstrate the application of MuTA for learning a universal set of gates, a measurement with classical post-processing, and a quantum instrument. Unlike earlier QML models in MBQC, MuTA combines features such as a being universal approximator, having tunable entanglement, being trainable in scale (with the right restrictions), and having engineerable bias. As discussed later, these attributes make the MuTA architecture a robust foundation for developing future QNN models within the MBQC paradigm.

II. MEASUREMENT-BASED QUANTUM MACHINE LEARNING

MBQC works by preparing an entangled state known as a *resource state* and then performing single-qubit measurements that consume this state [14]. Examples of re-

* luis@cs.toronto.edu

† polina.feldmann@ubc.ca

‡ dimbond@live.com

source states include graph states,

$$|G\rangle = \prod_{(i,j) \in E} CZ_{ij} |+\rangle^{\otimes n}. \quad (1)$$

Here, $G = (V, E)$ denotes a graph with vertices V and edges E , $X|+\rangle = |+\rangle$, and CZ is a Controlled- Z gate. X , Y , and Z are Pauli operators. To use $|G\rangle$ for MBQC, we define sets of input and output qubits $I, O \subset V$, respectively, together with single-qubit measurements M^i at each node $i \notin O$. A common choice, which we will assume in this paper, is $M_\alpha^i = \cos(\alpha)X_i + \sin(\alpha)Y_i$, $\alpha \in (-\pi, \pi]$. However, extended MBQC allows M_α^i to be in the (X, Z) and (Y, Z) planes, too [15]. The input of the circuit can be a quantum state $|\psi\rangle_{\text{in}}$, and in this case we replace the $|+\rangle$ qubits in I by $|\psi\rangle_{\text{in}}$ before applying the CZ gates in Eq. (1). If the input is classical, we can encode it in an input quantum state or in the measurement angles $\alpha(i)$ of M_α^i . The output of the circuit is stored in O .

To obtain a deterministic output in spite of the inherent randomness of quantum measurements, the measurement angles have to be conditioned on previous measurement outcomes. For MBQC on a graph state, the presence of *flow* guarantees a viable conditioning [16]. Let $N_G(i)$, $i \in V$ denote the neighbors of i in G . A resource state characterized by (G, I, O) has flow iff there exists a function $f : V \setminus O \rightarrow V \setminus I$ and a partial order $<$ such that $\forall i \in V$

- $(i, f(i)) \in E$,
- $i < f(i)$,
- $\forall j \in N_G(f(i)) \setminus \{i\} : i < j$.

The flow ensures that we can measure in a time order compatible with $<$ and compensate a (-1) -outcome on i by subsequently applying $X_{f(i)} \prod_{j \in N_G(f(i)) \setminus \{i\}} Z_j$. This compensation, which ensures determinism, is equivalent to a simple adaptation of measurement angles. To efficiently find the flow of a graph, we can use the algorithms presented in Refs. [17, 18]. There is a more general condition known as Pauli flow [15], which is necessary and sufficient for uniformly deterministic computation; however, for the sake of simplicity, we consider only graphs with flow.

Classical (supervised) machine learning aims to learn the underlying probability distribution of a given dataset. In the typical setup, a machine learning model \mathcal{M} is trained on a dataset $\mathcal{D} = \{(\mathbf{x}_i, y_i)\}_{i=1}^N$, where $\mathbf{x}_i \in \mathcal{X}$ represents features and $y_i \in \mathcal{Y}$ represents labels. The objective is to learn a function $f_\theta : \mathcal{X} \rightarrow \mathcal{Y}$, parameterized by θ , that approximates the true relationship between features and labels. This learning process is driven by a loss function $\ell(\theta; \mathcal{D})$, which evaluates the difference between predicted and true labels. During training, θ is optimized to minimize $\ell(\theta; \mathcal{D})$. The model's ability to generalize is tested on unseen data, reflecting its capabilities in representing the true data distribution.

Integrating the discussed concepts, an MBQC circuit with graph states as a resource is a tuple (G, I, O) together with a measurement pattern \mathcal{P}_θ which can be carried out deterministically. By allowing the measurement angles θ to be parameterized, we can define a QML model (also called ansatz) $\mathcal{E}_\theta : \mathcal{H}_I \rightarrow \mathcal{H}_O$ as the quantum channel defined by performing \mathcal{P}_θ with (G, I, O) on an input state $|\psi_{\text{in}}\rangle$ [19]. In general, a measurement-based quantum machine learning (MB-QML) model is a resource state together with a parametrized measurement pattern \mathcal{P}_θ that can deterministically perform inference on the input states of a given dataset $\mathcal{D} = \{(\rho_j, \sigma_j)\}_{j=0}^N$ and the parameters θ can be optimized to minimize a given loss function $\ell(\theta, \mathcal{D})$.

III. THE MULTIPLE-TRIANGLE ANSATZ

Classical deep neural networks (NNs) have shown an incredible power for learning to represent functions of real-world data. Several architectures have been proposed to solve problems with different structure, including multi-layer perceptrons, convolutional neural networks, transformers, graph neural networks, and many more. Common features these architectures share are the capability to (I) *universally approximate* functions with the desired structure, have a (II) *tunable message passing* between different nodes, have (III) *engineerable bias*, and (IV) *be trainable* at scale. Moreover, underlying all these complex models are a small set of operations that comprise an *artificial neuron*. A quest for QNN models has driven the community to propose many ideas for constructing circuits that behave similar to classical NNs [8, 20, 21].

Here, we introduce QNNs which are native to MBQC and exhibit a number of beneficial properties similar to those present in classical NNs. The centerpiece of our framework is a resource state constructed from simple, yet universal, building blocks inspired by Ref. [22]. Our *multiple-triangle ansatz* (MuTA) consists of 1D cluster states connected by multiple triangles as shown in Fig. 1. To navigate the qubits of this ansatz, we introduce the following sets: $Q_{i,k}$ denotes the qubit in row i and column k , $T_{i,j,k} = Q_{i,k} \cup Q_{j,k-1} \cup Q_{j,k} \cup Q_{j,k+1}$ is the set of qubits in a triangle connecting wires i (tip) and j (base) around column k , and $C_{i,j,k} := Q_{j,k} \subset T_{i,j,k}$ forms the center of its base. We denote $C_{i,j,k}$ and $T_{i,j,k}$ by $C_{i,j}$ and $T_{i,j}$ whenever k is unambiguous. To build MuTA layer (n, i) , we connect n wires of length 5 by a collection of triangles $T_{i,j,1}$ with $\{j\} \subseteq \{0, \dots, n-1\} \setminus \{i\}$ (note that we count starting from zero). We call a MuTA layer fully connected if $\{j\} = \{0, \dots, n-1\} \setminus \{i\}$. A MuTA consists of multiple MuTA layers. We concatenate two layers (n, i) and (n, j) of equal width n by identifying the output qubits O of the preceding with the input qubits I of the subsequent layer. When increasing (decreasing) n from one layer to the next, some of the input qubits of the second layer (output qubits of the first layer) join the

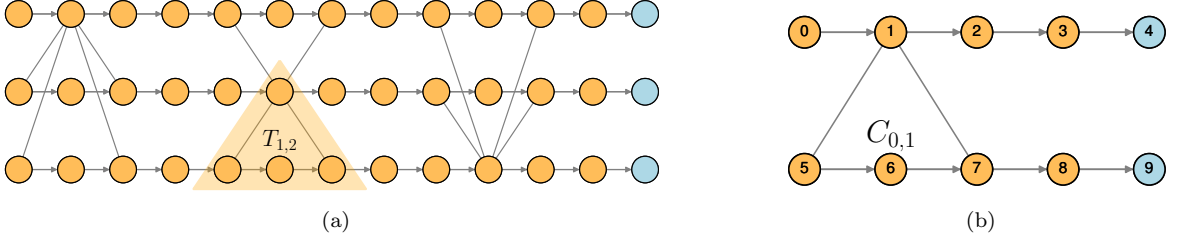


FIG. 1. Illustrations of the Multiple-Triangle Ansatz (MuTA) architecture: (a) A MuTA for three qubits, showing input qubits I on the left, output qubits O on the right (in blue), with arrows indicating the flow of (G, I, O) ; (b) A $(2, 0)$ -MuTA layer.

input (output) set of the overall graph state. We show that this architecture satisfies the following desiderata:

Property 1 (Determinism). *Any measurement pattern on MuTA can be performed deterministically.*

Proof. MuTA has a flow f defined by $f(Q_{i,k}) = Q_{i,k+1}$ for each node $i \in V \setminus O$. A compatible partial order $<$ is established as follows: $Q_{i,k} < Q_{i',k'}$ if either $k = k' = 4m$, $i \neq i'$ with $f(Q_{i,k})$ a tip qubit; $k = 4m$ and $k' = k + 1$ with $f(Q_{i,k})$ not a tip qubit; $k = k' = 4m + 1$, $i \neq i'$, and $Q_{i',k}$ a tip qubit; $k' = k + 1$ and $Q_{i,k}$ is a tip qubit; $k = 4m + 2$ and $k' = k + 1$; or $k = 4m + 3$, $k' = k + 1$, and $f(Q_{i',k'})$ is a tip qubit; additional relations are defined via transitivity. Thus, for any measurement pattern, Theorem 1 from Ref. [16] explicitly states how to adapt measurement angles to obtain a deterministic outcome. \square

Property 2 (Universality). *Given any n -qubit unitary operator $V \in U(2^n)$, there exists a measurement pattern on a sufficiently deep MuTA that exactly implements V .*

Proof. The set of single-qubit gates $V' \in U(2)$, together with an entangling gate such as $\text{IsingXX}(\varphi) = \exp(-i\varphi X \otimes X/2)$, forms a universal set of gates [23, 24], which implies any $V \in U(2^n)$ can be decomposed as product of these gates. Both types of gates can be implemented by MuTA using the measurement patterns shown in Table I. First, any single-qubit gate can be implemented by measuring a five-qubit wire with angles given by the Euler decomposition of $V' = R_x(-\lambda)R_z(-\phi)R_x(-\theta)$, where $R_x(\alpha) = \exp(-i\alpha X/2)$ and $R_z(\alpha) = \exp(-i\alpha Z/2)$ [14]. In addition, the $\text{IsingXX}(\varphi)$ gate can be implemented with a MuTA layer $(2, 0)$, which follows from the generator of $C_{i,j}$ (See Appendix A). Therefore, a MuTA layer of width n consisting of only n disconnected five-qubit wires can implement the former, while one consisting of $n - 2$ disconnected wires and a connected $(2, 0)$ block can implement the latter. Using combinations of these two layers with their corresponding measurement patterns we define a MuTA that exactly implement V . \square

Property 3 (Tunable Entanglement). *A fully connected MuTA layer (n, i) implements*

Gate	Measurement Pattern
$R_x(-\lambda)R_z(-\phi)R_x(-\theta) \otimes I$	$M_0^8 M_\lambda^3 M_0^7 M_\phi^2 M_\theta^1 M_0^6 M_0^5 M_0^0$
$\text{IsingXX}(\varphi)$	$M_0^8 M_0^3 M_0^7 M_0^2 M_0^1 M_\varphi^6 M_0^5 M_0^0$

TABLE I. Measurement patterns for universal gates in MuTA. Indices are matched with those from Figure 1b.

1. a non-entangling gate between wires i and $j \neq i$ if $C_{i,j}$ is measured at $\alpha \in \{0, \pi\}$
2. an entangling gate between wires i and $j \neq i$ if $C_{i,j}$ is measured at $\alpha \notin \{0, \pi\}$.

Proof. The first statement follows from noting that the only entangling generators of MuTA belong to $C_{i,j}$ qubits (see Appendix A), and these generate entanglement between wires i and j .

For the second statement, we recognize that all $C_{i,j}$ in the layer can be measured simultaneously (since $\forall j, j' C_{i,j} \not\leq C_{i,j'}$). This independence implies that the entanglement property between wires i and j does not depend on the measurement angle of $C_{i,j' \neq j}$. Consider $G_{i,k}$ to be the operation induced by measurement $M_\alpha^{C_{i,k}}$ on an input state. Then, there exist input states $|\psi\rangle_i, |\psi\rangle_j$ such that $G_{i,j}$ entangles subsystem i with j for $|\psi\rangle_{\text{in}} = \bigotimes_{k=0}^{|I|-1} |\psi\rangle_k$. Thus, for the input state $|\psi'\rangle_{\text{in}} = G_{ij'}^\dagger |\psi\rangle_{\text{in}}$ the operator $G_{ij} G_{ij'} |\psi'\rangle_{\text{in}}$ entangles subsystems i and j . \square

Property 4 (Monotonicity of Expressivity). *Adding layers or wires to a given MuTA does not restrict the implementable set of gates.*

Proof. Adding an additional MuTA layer or connecting an additional wire n by admissible triangles $T_{i,n}$ to existing layers (n, i) does not restrict the gates that can be expressed by the ansatz. An additional layer can always be turned into the identity operation by measuring all qubits in the X basis ($\alpha = 0$). For an additional wire, Property 3 directly implies that it can be disentangled without restricting the measurements on the other wires. \square

Property 5 (Bias Engineering). *The set of transformations implementable by a given MuTA depends on the chosen depth (number of layers), connectivity (triangles), preset or restricted measurement angles (variational parameters), and the width of intermediate layers (width variations generating auxiliary inputs and outputs).*

Proof. Straightforward from previous properties. \square

Property 6 (Scalability). *A fully connected MuTA with d layers of width n has $\leq 4 \times d \times n$ variational parameters.*

Proof. MuTA has at most as many variational parameters as qubits, i.e., $4 \times d \times n$. This number does not depend on connectivity. \square

Property 7 (2-Colorable). *The graph of any MuTA is 2-colorable.*

Proof. A graph is 2-colorable if and only if it is bipartite. Collecting all even columns into one subset and all odd columns into the other yields a bipartition of any MuTA. \square

These properties show MuTA possesses several features commonly found in classical NNs. Specifically, Properties 1-2 and 4 align with Feature (I), Property 3 with Feature (II), Property 5 with Feature (III), and Property 6-7 with Feature (IV). The last comparison is supported by the use of polynomial number of parameters and the existence of scalable purification protocols for constructing large MuTA [25]. Despite its advantages over other ansatzes with fixed entanglement structures, such as the cluster state, challenges persist. Notably, the quantum no-free lunch theorem [26] and the barren plateau phenomenon [27, 28] necessitate the tailoring of our ansatz to specific tasks and incorporating prior knowledge, such as the symmetries of the data [29], to achieve over-average performance and enable training at scale. These characteristics position MuTA as a promising universal QNN candidate within the MBQC framework.

IV. LEARNING TO MEASURE

In this section, we will explore multiple QML tasks and train the measurement angles from the MuTA (Figure 1b). We perform supervised learning on quantum data to learn a universal set of gates and study the effect of noise. We also perform classification of quantum states to distinguish between metrologically relevant and irrelevant quantum states, and we learn a quantum instrument that effectively implements teleportation between MuTA wires.

A. Universal set of gates

We show that the MuTA is universal by showing the sub-graph in Figure 1b can learn Haar-random local gates

in the first qubit and the entangling gate $\text{Ising}XX (\pi/2)$. The dataset used to learn the measurement angles is $\{\sigma_i, U\rho_i U^\dagger\}_{i=1}^N$ and the loss function to minimize is the average infidelity,

$$\ell(\theta) = 1 - \frac{1}{N} \sum_i F(\sigma_i, U\rho_i U^\dagger). \quad (2)$$

We use a dataset of size $N_{tr} = 7$ for training and $N_{te} = 3$ for testing, and use Haar-random states ρ_i for each datapoint. Then, using the Adam optimizer and average over 20 different random initializations and unitaries, we can learn this universal set of gates as shown in Figures 2a and 2b.

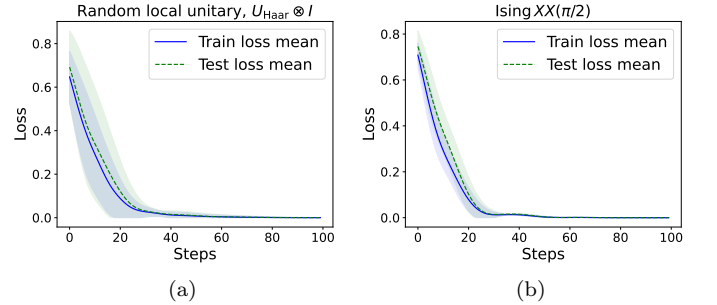


FIG. 2. Learning curves for the data sets for (a) single-qubit Haar-random unitaries in the first qubit and (b) an $\text{Ising}XX (\pi/2)$ gate. For (a), we average the learning curves obtained for 20 different unitaries. The shaded region is the standard deviation of the loss.

B. Learning with noise

A criterion for QML to be implementable in practice is robustness to environmental noise. We perform the same optimization routine made in Figure 2b for two noisy scenarios. First, training the model with noisy data $\{\sigma_i, \mathcal{N}(U\rho_i U^\dagger)\}_{i=1}^N$, and second, evolving the underlying graph state with a depolarizing channel, which we discuss in Appendix C.

For the noisy data case, we use a random unitary noise channel, defined as $\mathcal{N}_{rand}(\rho) = U_{br}^\dagger \rho U_{br}$, where U_{br} is the effect of a random Brownian circuit. This circuit can be constructed by evolving the system with random hermitian matrices H_i for a short amount of time $U_{br} = \prod_{j=0}^N e^{iH_i \Delta t}$. We also study the effect of a bit-flip noise channel at every qubit, $\mathcal{N}_{bit,j}(\rho) = (1-p)\rho + pX_j\rho X_j$.

In Figures 3a and 3b, we plot the optimized fidelity as a function of the noise strength after training for 60 and 200 steps, respectively. We averaged 5 learning curves that use a dataset of size $N_{tr} = 10$ for training and $N_{te} = 10$ for testing. Similar to the noiseless setting, each learning curve is obtained with a different Haar-random dataset. These figures show that increasing the noise strength reduces the fidelity of the trained circuit slowly, similar to

that seen in previous QNN proposals. For the bit-flip noise channel, the model can learn the correct parameters when the majority of the two-qubit dataset is not bit-flipped – this is, at $p < 0.5$.

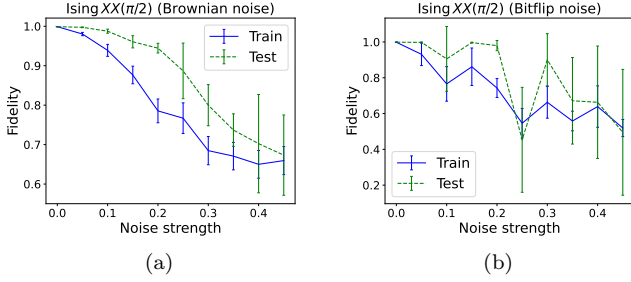


FIG. 3. Stability of QML routine under noise affecting the training dataset. The testing curves are obtained using noiseless datasets.

C. Measurement with classical post-processing

A field of application for QML is quantum sensing and quantum metrology [30–34]. Techniques in these fields use entangled states to better estimate an unknown parameter. Here, we train a hybrid quantum-classical model to distinguish between two-qubit states with high and low quantum Fisher information (QFI). This quantity is of great importance as it bounds the precision of any estimator of θ by the quantum Cramer-Rao bound $\text{Var}(\hat{\theta}) \geq \frac{1}{nF_Q(\theta)}$. In this problem, we deal with pure states ρ_θ , and for a given Hermitian Hamiltonian \hat{H} such that $\rho_\theta = e^{-i\theta\hat{H}}\rho e^{i\theta\hat{H}}$, the quantum Fisher information of a state is given by

$$F_Q(\rho_\theta) = 4 \left(\text{Tr}(\rho\hat{H}^2) - \text{Tr}(\rho\hat{H})^2 \right).$$

For our example, we set $H = h \otimes \mathbf{1} + \mathbf{1} \otimes h$ with $h = \alpha_x X + \alpha_y Y + \alpha_z Z$ and $\alpha_x^2 + \alpha_y^2 + \alpha_z^2 = \frac{1}{4}$ such that the *standard quantum limit* (SQL) and the *Heisenberg limit* (HL) become $F_Q^{(SQL)} = 2$ and $F_Q^{(HL)} = 4$, respectively. We use the value of F_Q to classify the states, which in the ideal case would be 0 for $F_Q(\rho) \leq 2$, and 1 otherwise.

We model $F_Q(\cdot)$ as a degree two polynomial in two variables $f_\beta(x_1, x_2) = \beta_0 + \beta_1 x_1 + \beta_2 x_2 + \beta_3 x_1^2 + \beta_4 x_1 x_2 + \beta_5 x_2^2$ (since F_Q is quadratic), together with the measurement angles θ of the MuTA, where x_1 and x_2 are the probabilities of outcomes (0, 0) and (1, 1) of the output state when measured in the (Z, Z) basis, respectively. Then, we optimize the parameters of the model $\hat{F}_\theta(\rho) := f_\theta(P_{00}, P_{11})$ by minimizing a soft-margin loss function

$$\ell(\theta) = \frac{1}{N} \sum_{i=1}^N \left[y_i \max \left\{ 0, -\hat{F}_\theta(\rho_i) + 2 + \epsilon \right\} + (1 - y_i) \max \left\{ 0, \hat{F}_\theta(\rho_i) - 2 + \epsilon \right\} \right],$$

where the parameter ϵ controls the width of the margin.

The input data used for training this POVM and classical post-processing model is a set of random states $S = S_1 \cup S_2$ sampled from a 2-parameter family,

$$S_1 = \{ \cos \theta |00\rangle + e^{i\phi} \sin \theta |11\rangle \mid \phi, \theta \sim \mathcal{U}_{[0, 2\pi]} \}$$

$$S_2 = \{ \cos \theta |++\rangle + e^{i\phi} \sin \theta |--\rangle \mid \phi, \theta \sim \mathcal{U}_{[0, 2\pi]} \},$$

where $\mathcal{U}_{[0, 2\pi]}$ is the uniform distribution and the target labels are 0 or 1 determined with the ideal classifier dictated by F_Q . This family of states is easy to prepare and spans a two-dimensional surface for every measurement basis.

We train this model using 50 states in S_1 and 50 in S_2 using the Adam optimizer and obtain a classifier with an accuracy of 0.9725 ± 0.0042 , where 0.0149 ± 0.0006 are false positives, and 0.0125 ± 0.0006 are false negatives, whenever we chose to ignore all states that have an estimated QFI between 1.9 and 2.1.

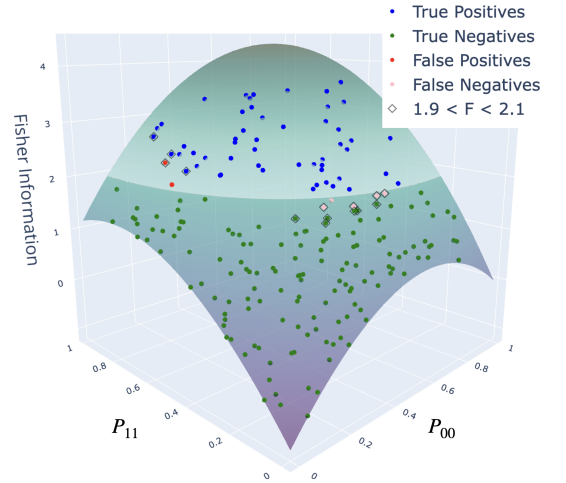


FIG. 4. Learned surface to classify states of high and low QFI. The surface is defined by a degree two polynomial, and the position of each point on the surface is defined by the measurement pattern.

The quantum Fisher information has a standard measurement protocol, making its estimation via QML seemingly redundant. But the main takeaway is showcasing MB-QML’s potential to classify states by metrics that aren’t directly measurable. This becomes invaluable when we can easily classify a subset of states using a known metric but struggle to do so for a larger set, particularly when an analytical expression for the metric is missing.

D. Quantum instrument for teleportation

Here we use MuTA with additional conditional measurements to learn a simple quantum instrument. In general, a quantum instrument is a map $\mathcal{I} : \text{End}(\mathcal{H}_1) \rightarrow$

$\text{End}(\mathcal{H}_2) \otimes \text{End}(\mathbb{C}^{|X|})$ that measures a state ρ and stores the measurement outcome,

$$\mathcal{I}(\rho) = \sum_{x \in X} E_x(\rho) \otimes |x\rangle\langle x|,$$

where $\{E_x\}_{x \in X}$ is a collection of completely positive maps such that $\text{Tr}(\sum_{x \in X} E_x(\rho)) = \text{Tr}(\rho)$. The instrument we study is the teleportation protocol. This protocol consists of creating a maximally entangled state $|\Phi\rangle$, measuring the state to be teleported $|\psi\rangle$ together with some subsystem of $|\Phi\rangle$ in an entangled basis, and finally applying a unitary transformation to the remaining unmeasured subsystem depending on the measurement outcome. The goal of this example is not to show that we can do teleportation, as the whole basis of MBQC is teleportation. The goal is to show that we can learn a quantum instrument using measurements conditioned to previous measurement outcomes.

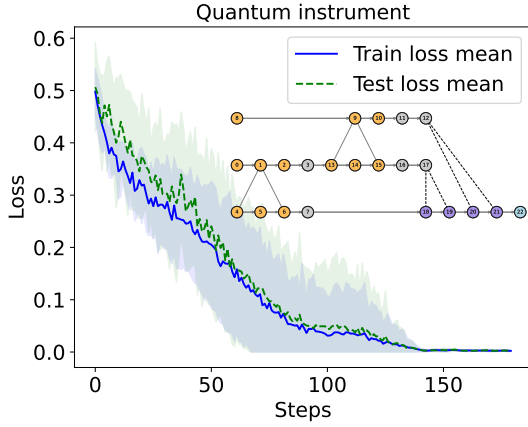


FIG. 5. Learning curve for learning an instrument that performs teleportation using the MuTA. We use different datasets of 35 states for training and 15 for testing in each run. We average over 10 learning curves. The node colors yellow, grey, purple, and light blue represent trainable, fixed, controlled, and quantum output nodes, respectively.

We can see in Figure 5 that the model learns the teleportation protocol from qubits 8 to 22 with a perfect fidelity, showing a proof-of-principle for learning quantum instruments with MB-QML.

E. Classification of classical data

Another application of MB-QML is the processing of classical data. Previously, there has been extensive work on using quantum models to classify classical datasets, and some examples can be found on [6, 9, 35]. Here, we show how to use MBQC to create a kernel Support Vector Machine (SVM) classifier and use it to classify synthetic datasets.

We again use MuTA, the universal ansatz we propose, to implement an embedding $x_i \mapsto |\phi(x_i)\rangle$ of a 2D dataset,

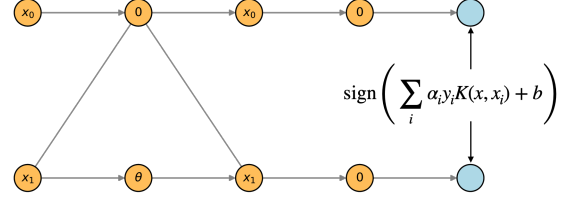


FIG. 6. Embedding used for kernel SVM classification of a 2D dataset. Here, the measurement angle θ is $\cos(x_0) \cos(x_1)$, where x_0 and x_1 are the coordinates of the input data.

shown in Figure 6. This map is used to construct the kernel which is discussed in more detail in Appendix D

$$K(x_i, x_j) = |\langle \phi(x_i) | \phi(x_j) \rangle|^2. \quad (3)$$

When classifying the different 'toy' datasets in Figure 7, we can see this kernel can be used for data that does not have a strongly non-linear structure, such as *circles* and *blobs*, but not for *moons*. This shows that there is room for improvement in the design of a quantum kernel using MBQC, possibly using kernel alignment, that can deal with datasets of higher dimensions and classify datasets with high degrees of non-linearity.

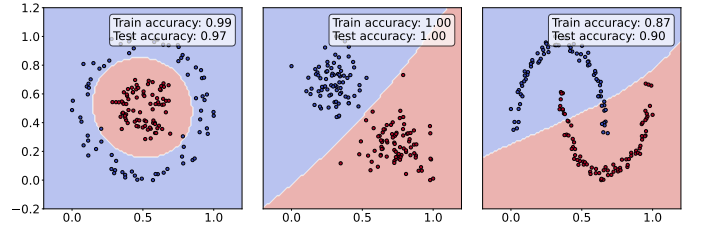


FIG. 7. The classification of three different datasets using the SVM with the kernel defined in Equations 3 and D1. All models were trained with 160 data points and tested with 40 data points.

V. HARDWARE-EFFICIENT ANSATZ

There are some hardware restrictions whenever implementing MBQC with photons. In particular, if we use the GKP encoding, measuring at arbitrary angles is complicated, whereas using the dual rail encoding, we can measure at arbitrary angles, but CZ gates are probabilistic [36, 37]. In terms of implementing a QML model with these restrictions, we have to learn to either use a discrete set of angles corresponding to accessible magic states or use a model with an underlying graph that changes every time. Here, we focus on the former and propose heuristic algorithms for discrete optimization over measurement patterns, where the possible angles are $\theta_i \in \{0, \pi/4, \pi/2\}$.

In this scenario of photonic GKP computation, measurements of 0 and $\pi/2$ can be performed using homodyne detection on the underlying graph state, while measurement in $\pi/4$ requires injecting a $|T\rangle := |0\rangle + e^{i\pi/4}|1\rangle$ magic state [38, 39].

Discrete optimization can be NP-hard. However, finding a heuristic for this hardware-constrained case can be of great practical value. We propose two different approaches to this problem. The first one is an epsilon-greedy algorithm that performs a layer-wise search over the measurement angles shown in Figure 8. The second is finding a pattern via deep Q-learning (DQN), a reinforcement learning (RL) algorithm, shown in Figure 9. The gate we chose to learn is $U = (T \otimes \mathbf{1}) e^{-i\frac{\pi}{8}X \otimes X}$, which requires T -magic states to be implemented [40]. Namely, we must inject $|T\rangle$ states in nodes 2 and 6 of Figure 1b. For the epsilon-greedy example, we used a dataset of $N = 10$, and for the DQN example, we used a dataset of $N = 30$, both with 30% of the data used for testing.

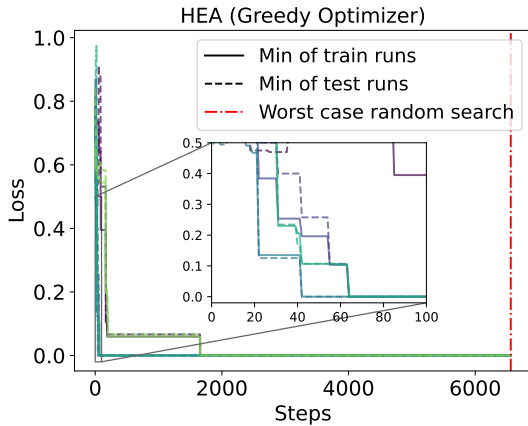


FIG. 8. Learning curves of five trials of the greedy algorithm compared to random search. All examples set $\epsilon = 0$ and $L_{max} = 4$. Two out of five runs got stuck in a local minimum until the parameters were reinitialized.

The second approach uses DQN to find the optimal measurement pattern. Here, the observation of the RL agent consists of the whole measurement pattern plus an additional node label input. The actions it can take are either measuring at an angle of 0, $\pi/2$, or $\pi/4$. Instead of searching for the best measurement angle at each node, the agent tries to find a balance between exploration and exploitation. This might lead to getting stuck in a local minimum, as shown in Figure 9. However, it's worth noting that the benefit of DQN would appear when there needs to be classical processing of partial information of the quantum state. This means if we measure some part of our state and extract information from it, DQN could learn how to use this classical information instead of the simple greedy search, which would naively suffer from the curse of dimensionality.

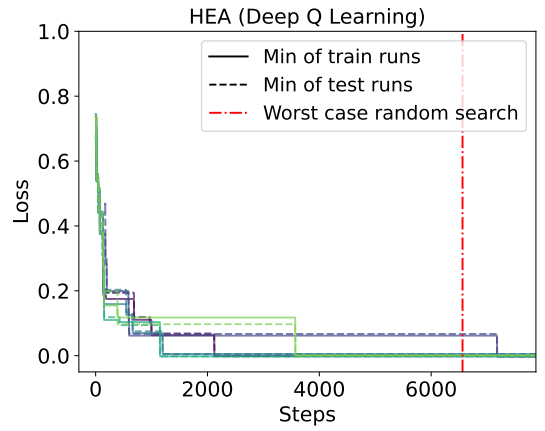


FIG. 9. Learning curves of five different runs using the DQN algorithm compared to random search.

VI. DISCUSSION

In this work, we studied how to use MBQC to do QML. In particular, we proposed and developed a framework for MB-QML. With this framework, we introduce a universal quantum neural network (MuTA) and demonstrated how to employ this ansatz to solve several tasks. MuTA is the first QNN in the MBQC framework that simultaneously satisfies desired properties mentioned in Section III, including being a universal approximator, having tunable entangling blocks, and permitting engineerable inductive bias. We provide numerical evidence for MuTA with experiments for learning a universal set of gates, a classifier of quantum states, and a quantum instrument. We also show how to do kernel SVM classification of classical data using the MuTA to create the kernel matrix and propose algorithms for optimization of MBQC circuits that are restricted by the hardware constraints of a photonic GKP qubit encoding.

Several questions arise from this work. An important question to ask is under which conditions on the data MB-QML performs better than its gate-based counterpart. It has been previously shown that using measurements with feedback can allow us to implement specific maps with fewer resources [1–3]. Thus, to exploit these benefits we would need a more elaborate model with classical and quantum processing that makes use of an MBQC ansatz. However, it would be ideal to find general conditions on arbitrary data distributions under which MB-QML would be better suited than gate-based QML.

Another promising area of research involves applying MB-QML to more complex datasets, including sequential quantum data. This could mean developing recurrent MB-QML models akin to those discussed in [41], or constructing mechanisms similar to attention models using graph states. The key approach here is to utilize measurements with feedback, as this technique seems to be crucial for enhancing the efficiency of computations.

ACKNOWLEDGMENTS

This work was funded by Canada First Research Excellence Fund and the Quantum Materials and Future Technologies Program. LM would like to thank helpful

discussions with Paul Herringer, Olivia Di Matteo, Ilan Tzitrin, and Alán Aspuru-Guzik.

Data availability: All simulations were made in Python, and they can be found in <https://github.com/mentpy/mentpy>.

-
- [1] M. Rossi, L. Asproni, D. Caputo, S. Rossi, A. Cusinato, R. Marini, A. Agosti, and M. Magagnini, Using shor's algorithm on near term quantum computers: a reduced version (2021), arXiv:2112.12647 [quant-ph].
 - [2] R. Raussendorf, S. Bravyi, and J. Harrington, Phys. Rev. A **71**, 062313 (2005).
 - [3] D. Malz, G. Styliaris, Z.-Y. Wei, and J. I. Cirac, Physical Review Letters **132** (2024).
 - [4] R. Raussendorf, D. E. Browne, and H. J. Briegel, Physical review A **68**, 022312 (2003).
 - [5] J. Biamonte, P. Wittek, N. Pancotti, P. Rebentrost, N. Wiebe, and S. Lloyd, Nature **549**, 195 (2017).
 - [6] A. Abbas, D. Sutter, C. Zoufal, A. Lucchi, A. Figalli, and S. Woerner, Nature Computational Science **1**, 403 (2021).
 - [7] I. Cong, S. Choi, and M. D. Lukin, Nature Physics **15**, 1273 (2019).
 - [8] K. Beer, D. Bondarenko, T. Farrelly, T. J. Osborne, R. Salzmann, D. Scheiermann, and R. Wolf, Nat Commun **11**, 808 (2020).
 - [9] M. Schuld and N. Killoran, Physical review letters **122**, 040504 (2019).
 - [10] J. Tilly, H. Chen, S. Cao, D. Picozzi, K. Setia, Y. Li, E. Grant, L. Wossnig, I. Rungger, G. H. Booth, *et al.*, Physics Reports **986**, 1 (2022).
 - [11] R. R. Ferguson, L. Dellantonio, A. Al Balushi, K. Jansen, W. Dür, and C. A. Muschik, Physical review letters **126**, 220501 (2021).
 - [12] W. J. Yun, H. Baek, and J. Kim, arXiv preprint arXiv:2210.16731 (2022).
 - [13] A. Majumder, M. Krumm, T. Radkohl, H. P. Nautrup, S. Jerbi, and H. J. Briegel, Variational measurement-based quantum computation for generative modeling (2023), arXiv:2310.13524 [quant-ph].
 - [14] R. Raussendorf and H. J. Briegel, Physical review letters **86**, 5188 (2001).
 - [15] D. E. Browne, E. Kashefi, M. Mhalla, and S. Perdrix, New Journal of Physics **9**, 250 (2007).
 - [16] V. Danos and E. Kashefi, Physical Review A **74**, 052310 (2006).
 - [17] N. De Beaudrap, Physical Review A **77**, 022328 (2008).
 - [18] M. Mhalla and S. Perdrix, in *Automata, Languages and Programming: 35th International Colloquium, ICALP 2008, Reykjavik, Iceland, July 7-11, 2008, Proceedings, Part I 35* (Springer, 2008) pp. 857–868.
 - [19] L. C. Mantilla Calderón, *Measurement-based quantum machine learning*, Master's thesis, University of British Columbia (2023).
 - [20] A. J. da Silva, T. B. Ludermir, and W. R. de Oliveira, Neural Networks **76**, 55 (2016).
 - [21] M. Benedetti, E. Lloyd, S. Sack, and M. Fiorentini, Quantum Science and Technology **4**, 043001 (2019).
 - [22] V. Danos, E. Kashefi, and P. Panangaden, Physical Review A **72**, 064301 (2005).
 - [23] M. A. Nielsen and I. L. Chuang, *Quantum computation and quantum information* (Cambridge university press, 2010).
 - [24] M. J. Bremner, C. M. Dawson, J. L. Dodd, A. Gilchrist, A. W. Harrow, D. Mortimer, M. A. Nielsen, and T. J. Osborne, Physical review letters **89**, 247902 (2002).
 - [25] K. Goyal, A. McCauley, and R. Raussendorf, Phys. Rev. A **74**, 032318 (2006).
 - [26] K. Poland, K. Beer, and T. J. Osborne, arXiv preprint arXiv:2003.14103 (2020).
 - [27] J. R. McClean, S. Boixo, V. N. Smelyanskiy, R. Babbush, and H. Neven, Nature communications **9**, 4812 (2018).
 - [28] M. Ragone, B. N. Bakalov, F. Sauvage, A. F. Kemper, C. O. Marrero, M. Larocca, and M. Cerezo, A unified theory of barren plateaus for deep parametrized quantum circuits (2023), arXiv:2309.09342 [quant-ph].
 - [29] L. Schatzki, M. Larocca, Q. T. Nguyen, F. Sauvage, and M. Cerezo, Theoretical guarantees for permutation-equivariant quantum neural networks (2022), arXiv:2210.09974 [quant-ph].
 - [30] C. L. Degen, F. Reinhard, and P. Cappellaro, Reviews of modern physics **89**, 035002 (2017).
 - [31] V. Giovannetti, S. Lloyd, and L. Maccone, Nature photonics **5**, 222 (2011).
 - [32] M. C. Caro, H.-Y. Huang, N. Ezzell, J. Gibbs, A. T. Sornborger, L. Cincio, P. J. Coles, and Z. Holmes, Nature Communications **14**, 3751 (2023).
 - [33] N. Li and S. Luo, Physical Review A **88**, 014301 (2013).
 - [34] P. Feldmann, *Generalized Quantum Phase Transitions for Quantum-State Engineering in Spinor Bose-Einstein Condensates*, Ph.D. thesis, Gottfried Wilhelm Leibniz Universität Hannover (2021).
 - [35] V. Havlíček, A. D. Córcoles, K. Temme, A. W. Harrow, A. Kandala, J. M. Chow, and J. M. Gambetta, Nature **567**, 209 (2019).
 - [36] E. Knill, R. Laflamme, and G. J. Milburn, Nature **409**, 46 (2001).
 - [37] P. J. Shadbolt, M. R. Verde, A. Peruzzo, A. Politi, A. Laing, M. Lobino, J. C. Matthews, M. G. Thompson, and J. L. O'Brien, Nature Photonics **6**, 45 (2012).
 - [38] E. Knill, Fault-tolerant postselected quantum computation: Schemes (2004), arXiv:quant-ph/0402171 [quant-ph].
 - [39] S. Bravyi and J. Haah, Physical Review A **86**, 052329 (2012).
 - [40] V. Danos, E. Kashefi, and P. Panangaden, Journal of the ACM (JACM) **54**, 8 (2007).
 - [41] D. Bondarenko, R. Salzmann, and V.-S. Schmiesing, arXiv preprint arXiv:2301.08167 (2023).
 - [42] Y. Suzuki, H. Yano, Q. Gao, S. Uno, T. Tanaka, M. Akiyama, and N. Yamamoto, Quantum Machine Intelligence **2**, 1 (2020).

datapoint x . In Figure 6, we get the map

$$|\phi(x_i)\rangle = R_{z1}(x_{i2})R_{z0}(x_{i1})e^{-i\cos(x_{i1})\cos(x_{i2})X\otimes X} \\ \times R_{z1}(x_{i2})R_{z0}(x_{i1})|00\rangle. \quad (\text{D1})$$

Experimentally, each entry of K can be obtained using a swap test. This means that to get $K(x_i, x_j)$ we need two graph states to prepare $|\phi(x_i)\rangle$ and $|\phi(x_j)\rangle$, and get enough samples from the overlap to estimate $|\langle\phi(x_i)|\phi(x_j)\rangle|^2$. This kernel is inspired by a previous embedding studied in [42].

Appendix E: Hardware efficient training algorithms

In Section V, we used heuristic algorithms to get the optimal measurement angles from a discrete set of angles. In particular, those accessible in a GKP encoding with T -magic state injection. The first algorithm we use is Algorithm 1.

Algorithm 1 Layer-wise greedy search algorithm for discrete optimization of measurement patterns.

```

1: function GREEDYOPT( $\ell, \varepsilon, A, \text{layers}, n_{\text{reset}}, L_{\text{max}}, \delta$ )
2:   for  $\text{reset} = 0$  to  $n_{\text{reset}}-1$  do
3:     for  $m = 1$  to  $L_{\text{max}}$  do
4:        $A = \text{LayerOpt}(\ell, A, \text{layers}, m, \varepsilon)$ 
5:       if  $\ell(A) < \delta$  then
6:         return True,  $A$ 
7:       else
8:          $A = \text{randomAngles}()$ 
9:   return False,  $A$ 
10: function LAYEROPT( $\ell, A, \text{layers}, n, \varepsilon$ )
11:   for  $i = 0$  to  $\text{len}(\text{layers}) - n$  do
12:      $\text{merged\_layers} = \text{concatenate}(\text{layers}[i:i+n])$ 
13:      $A_{\text{best}} = A$ 
14:      $\ell_{\text{best}} = \ell(A)$ 
15:     for all  $A' \in \{0, \pi/4, \pi/2\}^{\text{merged\_layers}}$  do
16:        $\ell_{\text{current}} = \ell(A')$ 
17:       if  $\ell_{\text{current}} < \ell_{\text{best}}$  or  $\text{random}(0, 1) < \varepsilon$  then
18:          $A_{\text{best}} = A'$ 
19:          $\ell_{\text{best}} = \ell_{\text{current}}$ 
20:   return  $A_{\text{best}}$ 

```

The second algorithm we used was DQN, a popular reinforcement learning algorithm suitable for discrete state and action spaces. In this context, the state space (or observation) includes the entire measurement pattern, along with a node label j indicating which node the agent will modify next. The action space consists of selecting a measurement angle at j from the set $0, \pi/2, \pi/4$. This approach helps balance exploration and exploitation, and depending on the model's hyperparameters, it may converge to a global or local minimum of the loss.